Enhanced Raman scattering by fractal clusters: Scale-invariant theory

Mark I. Stockman*
Departments of Physics and Chemistry, Washington State University, Pullman, Washington 99164

Vladimir M. Shalaev† and Martin Moskovits
Department of Chemistry, University of Toronto, and Ontario Laser and Lightwave Research Center, Toronto, Ontario, Canada M5S 1A1

Robert Botet
Laboratoire de Physique des Solides, Université Paris-Sud, Centre d'Orsay, 91405 Orsay, France

Thomas F. George
Departments of Physics and Chemistry, Washington State University, Pullman, Washington 99164
(Received 28 January 1992)

A scale-invariant theory of Raman scattering of light by fractal clusters is developed. The enhancement factor G^{RS} of Raman scattering is shown to scale in terms of a properly chosen spectral variable X. The critical indices of the enhancement factor are found to be determined by the optical spectral dimension of the fractal. Numerical modeling is carried out and shown to support the analytical results obtained. The theory, which does not contain any adjustable parameters, agrees well with experimental data on surface-enhanced Raman scattering over a wide spectral range.

I. INTRODUCTION

Surface-enhanced Raman scattering (SERS) is one of the most intriguing optical effects discovered[1,2] in the past 15 years. Its manifestation is a very great increase, often as large as a 10^6-fold, in the Raman-scattering intensity of molecules absorbed on the surfaces of special metallic structures, as compared to the intensity of an equivalent number of molecules in solution or the gas phase. The special metallic structures that display SERS normally involve small metal features such as those found on microrough metal surfaces and in aggregated colloidal particles, whose dimensions are much smaller than wavelength λ. The major contribution to the enhancement is understood to originate from the large local electromagnetic fields that arise from resonant optical excitation of surface plasmons. Because these plasmons are both intense (i.e., possessing great dipole moments and low decay rates) and easily excitable with commonly available laser sources for the alkali and coinage metals, the SERS effect is largely restricted to these metals.

Theory shows that field enhancement can be great at the points of high curvature (the so-called lightning rod effect).[3] However, the most effective SERS systems are collections of interacting particles. The reason for this is understood to be even greater field enhancement that results from electromagnetic interactions among the constituent small metal particles. Models have been reported that account for these interactions in terms of the modifications of the Lorentz local field operating on a particle due to the presence of neighboring particles.[4] However, the mean concentration of metal needed in these treatments to achieve the red shifts observed experimentally is much too high. Additionally, Aravind, Nitzan, and Metiu have calculated[5] the magnitude of the electromagnetic field at various locations in the vicinity of two interacting particles invoking very high multipoles. Also, Liver, Nitzan, and Gersten have reported[6] the results of a calculation among several metal particles, but restricting the interaction to dipole-dipole. These calculations demonstrate that, in addition to a further increase in the local field magnitude, the interaction among particles also results in a red shift of the maximum enhancement wavelength from the surface plasmon resonance positioned in the near uv. However, none of the above-mentioned theories can satisfactorily explain the form of the spectral contour of SERS, which is very wide with the maximum enhancement in the red region.

Although the precise structure of roughened metal surfaces is not known with certainty, the structure of colloid aggregates has been investigated by various methods and shown to be fractal (see, e.g., the electron microscopy study of Ref. 7). The Hausdorff dimension D of such aggregates is consistent with that characteristic of cluster-cluster aggregation.[7–9] For the sake of brevity, we will refer to fractal clusters simply as fractals. This should not cause confusion because no other physical realizations of fractals will be discussed.

A tentative theory of enhanced Raman scattering by fractals has already been considered.[10] Because it is based on a binary approximation, this treatment is only applicable to diluted fractals, making it unable to account for the form of either the absorption spectrum or the Raman excitation contour. A scale-invariant theory has been developed in Ref. 11 to describe the linear optical polarizability of fractals. It demonstrates the scaling properties of the absorption and determines the dispersion relation for the dipolar excitation modes of the fractal (see also

Ref. 12). The important qualitative features of scaling are the dominance of the strong fluctuations of local fields at all scales and a significant restriction in the spatial extent of the eigenmodes to small regions within the cluster. Such localization for the fractal vibrations ("fractons") has been predicted[13] by Alexander and Orbach, and experimentally observed[14] recently by Sapoval, Gobron, and Margolina for acoustic excitation of fractal drums.

A scale-invariant theory developed by Alexander[15] describes Raman scattering from vibration modes of fractals. However, this theory does not include dipolar excitations (plasmons) and, therefore, cannot describe the phenomenon of SERS. In the present paper, we develop a scale-invariant theory of SERS from fractals which is insensitive to details of the cluster structure providing universal description of this phenomenon in terms of a few critical exponents. The present theory fully takes into account the strong spatial fluctuations of local fields characteristic of fractals and their excitations. It is capable of explaining both the magnitude and spectral contour of the enhancement.

In Sec. II we formulate the model and basic equations governing linear response of the fractal. In Sec. III general expressions for the enhancement factor G^{RS} are obtained, and self-similarity is invoked to derive the scaling expressions for G^{RS}. Numerical simulation with the use of the Monte Carlo method in Sec. IV confirms the predictions of the scaling theory. The results are discussed and shown to be in a good agreement with experimental data in Sec. V.

II. FORMULATION OF THE MODEL AND LINEAR RESPONSE OF A CLUSTER

Let us very briefly recapitulate the formulation of the model and the results for the linear optical response of fractals (Ref. 11), which are necessary for the present paper. A fractal is considered as a system of N polarizable particles (monomers) with dipole-dipole interaction between them at optical frequencies. The monomers are positioned at points $\mathbf{r}_i$, $i=1,\ldots,N$. The number N of monomers in a fractal scales as

$$N\sim(R_c/R_0)^D\ , \tag{1}$$

where D is an index called the Hausdorff dimension, R_c is a characteristic total size of the fractal, and R_0 is a constant equal to a typical separation between monomers. A fractal is called nontrivial if $D<3$. The length R_0 plays the role of a minimum scale of the fractal, and the dependence on R_0 is of principal importance to the theory (see Ref. 11 and below).

Since Raman scattering is accompanied by a Stokes frequency shift, the linear response of the cluster at the frequency ω of the exciting radiation can be found independently from its Raman response at the shifted frequency ω_s. Experimentally, most fractal clusters are larger than the exciting wavelength λ. However, the localization (coherence) length of fractal excitations can be much smaller than λ. Also, under certain conditions, the interaction of monomers at distances greater than λ can be neglected. We will find qualitative conditions for the validity of the two assumptions at the end of the next section [see Eqs. (39) and (40)].

Accepting these assumptions, one can neglect the spatial variation of the electric field $\mathbf{E}^{(0)}$ of the exciting optical wave and obtain the well-known system of equations describing the transitional dipole moment $\mathbf{d}_i$, induced on the ith monomer (oscillating with frequency ω),

$$Zd_{i\alpha}=E^{(0)}_{\alpha}-\sum_{j=1}^{N}(i\alpha|W|j\beta)d_{j\beta}\ , \tag{2}$$

where $i=1,\ldots,N$. Here $Z=\chi_0^{-1}$, χ_0 is the linear polarizability of a monomer at the light frequency ω, and W is the dipole interaction tensor,

$$(i\alpha|W|j\beta)=\begin{cases}[\delta_{\alpha\beta}-3n^{(ij)}_{\alpha}n^{(ij)}_{\beta}]r_{ij}^{-3}, & i\neq j\\ 0, & i=j\ .\end{cases} \tag{3}$$

The Greek indices label tensor components, summation over repeated Greek indices is implied, $\mathbf{r}_{ij}=\mathbf{r}_i-\mathbf{r}_j$, and $\mathbf{n}^{(ij)}=\mathbf{r}_{ij}/r_{ij}$. Of course, Eq. (2) is quantitatively applicable to small clusters ($R_c\ll\lambda$) without invoking additional assumptions discussed above.

We shall reformulate the system (2) as an equation in $3N$-dimensional linear space, introducing the vector $|d)$ with components $(i\alpha|d)=d_{i\alpha}$, and similarly for other vectors. In this way, we obtain

$$Z|d)=|E^{(0)})-W|d)\ , \tag{4}$$

where W is the operator determined by its matrix elements (3).

Let us introduce the eigenvectors $|n)$ of the W operator and the corresponding eigenvalues w_n: $(n|W|m)=w_n\delta_{nm}$, where $n,m=1,2,\ldots,3N$. Note that the eigenvalues w_n and components of the eigenvectors $(i\alpha|n)$ are all real due to the symmetry of W. The solution of Eq. (4) in the $|n)$ basis has the form

$$(n|d)=(n|E^{(0)})\Lambda_n,\quad \Lambda_n\equiv(Z+w_n)^{-1}\ . \tag{5}$$

From Eq. (5), the expression of Ref. 11 for the polarizability tensor χ_i of the ith monomer in the cluster can be obtained as[16]

$$\chi_{i,\alpha\beta}=\sum_{n,j}\Lambda_n(i\alpha|n)(j\beta|n)\ . \tag{6}$$

The local field E_i acting on the ith monomer can easily be expressed as

$$E_{i\alpha}=\chi_0^{-1}\chi_{i,\alpha\beta}E^{(0)}_{\beta}\ . \tag{7}$$

After averaging over the orientation of a cluster as a whole, the polarizability tensor is reduced to a scalar

$$\chi=\tfrac{1}{3}\langle\chi_{i,\alpha\alpha}\rangle\ , \tag{8}$$

where $\langle\ \rangle$ indicates averaging over the ensemble of clusters. The total absorption cross section σ_a of the cluster is proportional to $\mathrm{Im}\chi$, namely, $\sigma_a=4\pi kN\,\mathrm{Im}\chi$, where k is the light wave vector. Below we will refer to $\mathrm{Im}\chi$ simply as the absorption.

The exciting light frequency ω enters Eq. (4) and subsequent expressions implicitly, via the complex variable Z.

Also, all material and geometrical properties of monomers affect the problem only through Z. Let us isolate the real and imaginary parts of Z in the form $X=-\mathrm{Re}Z$, $\delta=-\mathrm{Im}Z$. The quantity X plays the role of a spectral variable in place of ω, and the parameter $\delta>0$ describes the dissipation in a monomer. The dependence of both X and δ on ω for real systems is discussed in Sec. V.

Another quantity of fundamental importance for the theory is the density $\nu(X)$ of fractal eigenmodes per monomer defined as

$$\nu(X)=N^{-1}\left\langle \sum_n \delta(X-w_n) \right\rangle . \tag{9}$$

The absorption and eigenmode density satisfy the exact sum rules[11]

$$\int_{-\infty}^{\infty} \mathrm{Im}\chi(X)dX=\pi, \quad \int_{-\infty}^{\infty} \nu(X)dX=3 . \tag{10}$$

The principal advantage of using X is shown in Ref. 11 to be due to the fact that optical responses scale with X but not with ω. In particular, $\mathrm{Im}\chi(X)$ and $\nu(X)$ have identical scaling,

$$\mathrm{Im}\chi(X)\sim\nu(X)\sim R_0^3(R_0^3|X|)^{d_o-1} . \tag{11}$$

Here d_o is a critical index introduced in Ref. 11, which governs the properties of optical responses of fractals and is called the optical spectral dimension. It plays a similar role for polar excitations of fractals as Alexander and Orbach's index,[13] fracton dimension $\bar{\bar{d}}$, does for vibrational excitation. However, in contrast to $\bar{\bar{d}}$, the physical range for d_o is $0<d_o<1$. The condition of scaling has the form[11]

$$\delta, R_0^{-3}N^{-(3/D-1)/(1-d_o)} \ll |X| \ll R_0^{-3} . \tag{12}$$

For X in this region, the light excites collective modes of the fractal, i.e., modes delocalized over many monomers. However, these modes are still well localized within the whole fractal. In other words, the coherence length L_X of the excitations,[11]

$$L_X\sim R_0(R_0^3|X|)^{-(1-d_o)/(3-D)} , \tag{13}$$

conforms to the inequality $R_0\ll L_X\ll R_c$. Due to this, the optical responses of the fractal per monomer do not depend either on the fractal fine structure or on the total number of monomers N.

Since there is no dependence on the fractal fine structure in the range given by Eq. (12), we can always unify some number of nearest monomers into a composite particle and call it a new (renormalized) monomer. Such a renormalization transformation changes only the fractal structure on a minimum scale; in particular, the length R_0 is changed. The total absorption of the fractal should not change under the renormalization transformation, which means that $\sigma_a\propto R_0^0$. From this and Eq. (11), a transformation law[11] follows,

$$|X|\propto R_0^{(3d_o-D)/(1-d_o)} . \tag{14}$$

III. ENHANCED RAMAN SCATTERING BY CLUSTERS

We assume that each monomer of the cluster apart from the linear polarizability χ_0 possesses also Raman polarizability κ. The exciting field $\mathbf{E}$ applied to an isolated monomer, therefore, induces a dynamic dipole moment $\mathbf{d}^s$ oscillating with the Stokes-shifted frequency ω_s. In order to avoid unnecessary complications, κ will be assumed to be scalar. Accordingly, we have $\mathbf{d}^s=\kappa\mathbf{E}$. The Raman polarizability may be either the polarizability of a monomer itself or that of adsorbed molecules bound to the monomer.

For spontaneous Raman scattering, which is an incoherent optical process, the Raman polarizabilities κ_i of different monomers ($i=1,2,\ldots,N$) contain uncorrelated random phases. This can be expressed as

$$\langle \kappa_i^*\kappa_j\rangle=|\kappa|^2\delta_{ij} . \tag{15}$$

This feature constitutes the principal difference between κ and the linear polarizability χ_0, ensuring that there will be no interference between the Stokes waves generated by different monomers.

The field acting upon an ith monomer in a cluster is the local field $\mathbf{E}_i$ rather than the external field $\mathbf{E}^{(0)}$. Likewise, it is the dipole interactions of the monomers at the Stokes-shifted frequency ω_s that should be considered. The components of $\mathbf{d}^s$ obey, therefore, the following system of equations:

$$d_{i\alpha}^s=\kappa_i E_{i\alpha}-\chi_0^s\sum_{j,\beta}(i\alpha|W|j\beta)d_{j\beta}^s , \tag{16}$$

where χ_0^s is the linear polarizability of an isolated monomer at the Stokes-shifted frequency ω_s. Equations (16) can be rewritten as a vector equation in $3N$-dimensional space

$$|d^s)=\hat{\kappa}|E)-\chi_0^s W|d^s) , \tag{17}$$

where $\hat{\kappa}$ is an operator defined by its matrix elements

$$(i\alpha|\hat{\kappa}|j\beta)=\kappa_i\delta_{ij}\delta_{\alpha\beta} . \tag{18}$$

The formal solution to Eq. (17) has the form

$$|d^s)=\frac{Z_s}{Z_s+W}\hat{\kappa}|E) , \tag{19}$$

where $Z_s\equiv(\chi_0^s)^{-1}$. Combining Eqs. (4) and (19), one obtains

$$|d^s)=\frac{Z_s}{Z_s+W}\hat{\kappa}\frac{Z}{Z+W}|E^{(0)}) . \tag{20}$$

Using the completeness of vector sets $|n)$ and $|i)$, we rewrite (20) in the form

$$d_{i\alpha}^s=Z_s Z\sum_{n,n',j,j'}\kappa_j\Lambda_n^s\Lambda_{n'}(i\alpha|n)(j\beta|n)\times(j\beta|n')(j'\beta'|n')E_{\beta'}^{(0)} . \tag{21}$$

Using Eq. (6) to clear the matrix elements from (21), we obtain the following expressions for the total Stokes dipole moment $\mathbf{D}^s$ of the cluster:

$$D^s_\alpha=\sum_i d^s_{i\alpha}=Z_s Z\sum_j \kappa_j \chi^s_{j,\beta\alpha}\chi_{j,\beta\beta'}E^{(0)}_{\beta'} , \tag{22}$$

where $\chi^s_j=\chi_j(X_s)$, as given by Eq. (6) with substitution of $X_s=-\mathrm{Re}Z_s$ for X, is the polarizability of the jth monomer in the cluster at frequency ω_s.

The enhancement factor of SERS is given by

$$G^{\mathrm{RS}}=\frac{\langle|\mathbf{D}_s|^2\rangle}{N|\kappa|^2|\mathbf{E}^{(0)}|^2} . \tag{23}$$

This factor expresses increase in the Raman intensity of light scattered by a fractal cluster consisting of N monomers with respect to the integral Raman intensity of light scattered by N separate (nonaggregated) monomers.

Expressions (16)–(23) are valid for clusters of any geometry, fractal or not. To find a closed-form expression for G^{RS}, we must invoke the concept of scaling as well as some approximations. First, we consider the case of the Stokes shift so large that the Raman-scattered light is well out of the absorption band of the fractal. This requires, in particular, that $R_0^3|X-X_s|\gg 1$. In this case, the polarizability (6) at frequency ω_s is expressed as $\chi^s_{i,\alpha\beta}\approx Z_a^{-1}\delta_{\alpha\beta}$. Substituting this into Eq. (22), after averaging over all orientations, we obtain from Eq. (23)

$$G^{\mathrm{RS}}=|Z|^2\frac{1}{3N}\left\langle\sum_i|\chi_{i,\alpha\beta}|^2\right\rangle . \tag{24}$$

The exact relation $\sum_i\chi_{i,\alpha\beta}\chi_{i,\alpha\gamma}=\delta^{-1}\sum_i\mathrm{Im}\chi_{i,\alpha\beta}$ has been proved in Ref. 11, based on the completeness of the eigenvector set $(i\alpha|n)$. Substituting this into Eq. (24) and taking account of Eq. (7), we finally obtain

$$G^{\mathrm{RS}}=\delta(1+X^2/\delta^2)\mathrm{Im}\chi . \tag{25}$$

This expression for G^{RS} coincides exactly with the expression found previously [see Eq. (20) in Ref. 11] for the enhancement factor G of the local field fluctuations. This is expected, because in the limiting case considered, the Raman-scattered light does not interact with the fractal, and the Raman-scattering intensity is simply proportional to the mean square of the local fields. The exact expression (25) reduces in the scaling region to the form

$$G^{\mathrm{RS}}\simeq X^2\delta^{-1}\mathrm{Im}\chi\sim Q(R_0^3|X|)^{d_o+1} , \tag{26}$$

where $Q\equiv(R_0^3\delta)^{-1}$ is a large dimensionless parameter [cf. Eq. (12)] which plays the role of the resonance quality factor for the monomer.

If the Stokes shift is not very large, the general expression for G^{RS} is needed, which follows from Eqs. (6), (22), and (23) after averaging over the orientations,

$$G^{\mathrm{RS}}=\frac{1}{3N}|Z_sZ|^2\left\langle\sum_{n,n',m,m'}K_{nn'mm'}\Lambda^{(s)}_n\Lambda_{n'}\Lambda^{(s)*}_m\Lambda^*_{m'}\right\rangle , \tag{27}$$

where the kernel K is defined as

$$K_{nn'mm'}=a_{n\alpha}a_{n'\beta}a_{m\alpha}a_{m'\beta}\times\sum_j(j\gamma|n)(j\gamma|n')(j\delta|m)(j\delta|m') , \tag{28}$$

with $a_{n\alpha}\equiv\sum_i(i\alpha|n)$. The completeness and orthogonality of the eigenvectors $|n)$ ensures that the kernel K satisfies the sum rule

$$\sum_{n,n',m,m'}K_{nn'mm'}=3N . \tag{29}$$

Expression (27) cannot be evaluated analytically in a general form. Instead, we will consider the limiting case of an extremely small Stokes shift, $|X-X_s|\ll\delta$, which is experimentally satisfied for most Raman bands. Then the Stokes shift can be neglected in Eq. (27), and one can set $Z=Z_s$, $\Lambda=\Lambda^s$. In the scaling region (12), we can set $|Z|=|X|$ to a high degree of accuracy. Taking this into account, we obtain from Eq. (27)

$$G^{\mathrm{RS}}=\frac{1}{3N}X^4g(X),\ g(X)\equiv\left\langle\sum_{n,n',m,m'}K_{nn'mm'}\Lambda_n\Lambda_{n'}\Lambda^*_m\Lambda^*_{m'}\right\rangle . \tag{30}$$

To further evaluate G^{RS}, we will invoke scale invariance and employ the sum rule approach. An exact sum rule for the function $g(X)$ (30) has the form

$$\int_{-\infty}^{\infty}g(X)dX=-2\pi\,\mathrm{Im}\left\langle 2\sum_{n,n',m,m'}K_{nn'mm'}R_{nm}R_{n'm'}\times(R_{nm'}+R_{n'm})\right\rangle , \tag{31}$$

where

$$R_{nm}=(w_n-w_m-2i\delta)^{-1} . \tag{32}$$

The sum rules (10) are satisfied, on the order of magnitude, if we use $\mathrm{Im}\chi(X)$ and $\nu(X)$ in the scaling approximation (11) and expand the integrals over the scaling region, $|X|\lesssim R_0^{-3}$. This means that the number of eigenmodes contained in the scaling region (12) is on the order of the total number $3N$ of eigenmodes. Because the integral in Eq. (31) is rapidly converging, it is plausible that the integration over the scaling region gives the major contribution to it. In that case, $\int g(X)dX$ would be scale invariant. This is what we will assume. The scale invariance assumption is strongly supported by numerical results (see below). The integral $\int g(X)dX$ must be proportional to N, in order to yield G^{RS} independent of N [see Eq. (30)]. Therefore its scale invariance means that $N^{-1}\int g(X)dX$ depends on neither R_0 nor R_c and can be expressed in terms of δ only. Taking the dimensionality into account, we obtain the simple estimate $\int g(X)dX\sim N\delta^{-3}$. Comparing this relation with Eq. (31), we arrive at the conclusion that in Eq. (32) $|w_m-w_n|\ll\delta$ in the essential region of integration in Eq. (31). In this case, neglecting the difference of eigenvalues in Eq. (32) and taking Eq. (29) into account, we obtain from Eq. (31) the sum rule

$$\int_{-\infty}^{\infty}g(X)dX\simeq\frac{3\pi}{2}\frac{N}{\delta^3} . \tag{33}$$

Considering the dimensionality arguments, the scaling expression for $g(X)$ follows from Eq. (33),

$$g(X)\sim NR_0^3\delta^{-3}(R_0^3|X|)^\theta , \tag{34}$$

where θ is an index. The scale invariance of $g(X)$ implies that under the renormalization transformation

$g(X) \propto R_0^0$. From this requirement and taking into account transformation law (14) and Eq. (1), we immediately obtain $\theta = d_o - 1$. This gives us the scaling form

$$G^{\mathrm{RS}} \sim Q^3 (R_0^3 |X|)^{d_o + 3} . \tag{35}$$

The coefficient of the asymptotic dependence in Eq. (35) can be estimated using sum rules (10) and (33). Taking account of the scaling relation (11), we can rewrite Eq. (34) as $g(X) \sim N R_0^3 \delta^{-3} \mathrm{Im}\chi(X)$. As comparison with Eq. (10) shows, sum rule (33) is satisfied if the coefficient in this relation is chosen to equal $\frac{3}{2}$, yielding

$$G^{\mathrm{RS}} \approx \tfrac{1}{2} Q^3 (R_0^3 X)^4 \mathrm{Im}\chi(X) . \tag{36}$$

Because relations (35) and (36) are the final results and of principal importance, let us indicate another way of obtaining them. The product of the Λ factors in Eq. (27) can be rewritten identically as

$$\begin{aligned} \Lambda_n \Lambda_{n'} \Lambda_m^* \Lambda_{m'}^* = R_{nm} R_{n'm'} [& \Lambda_n \Lambda_{n'} + \Lambda_m^* \Lambda_{m'}^* \\ & + R_{nm'} (\Lambda_n - \Lambda_{m'}^*) \\ & + R_{mn'}^* (\Lambda_m^* - \Lambda_{n'})] . \end{aligned} \tag{37}$$

To yield the scaling form of G^{RS}, the difference of the eigenvalues in Eq. (37) should be negligible with respect to δ. Assuming scaling and neglecting this difference, as was done above, and using the orthonormality relation of the eigenvectors, we obtain from Eq. (27)

$$G^{\mathrm{RS}} \approx \frac{1}{6N\delta^3} X^4 \left\langle \sum_n a_{n\alpha}^2 \mathrm{Im}\Lambda_n \right\rangle . \tag{38}$$

Taking Eqs. (6) and (8) into account, we see that Eq. (38) is equivalent to Eq. (36).

Let us emphasize that in the case of a large Stokes shift, expression (26) for G^{RS} is asymptotically exact, i.e., both the scaling index $d_o + 1$ and the proportionality coefficient are correct. In the case of a small Stokes shift, we believe that the index $d_o + 3$ in Eq. (35) is also asymptotically exact because it is derived from the general requirements of scale invariance. Unlike it, the numerical coefficient $\frac{1}{2}$ in Eq. (36) is only an estimate, its accuracy depending on what fractions of the sum rules (10) and (33) are saturated in the scaling region (12).

The scale-invariant theory presented above is developed based on Eq. (2), where the spatial variation of the exciting field $\mathbf{E}^{(0)}$ is neglected. A necessary condition for the validity of such neglect and also for the existence of scaling is $L_X \ll \lambda$, which, upon taking account of Eq. (13), acquires the form

$$R_0^3 |X| \gg (R_0/\lambda)^{(3-D)/(1-d_o)} . \tag{39}$$

This condition does not contradict Eq. (12), because it is assumed that $R_0 \ll \lambda$, as is the case experimentally (note that $D < 3$ and $d_o < 1$).

To have the indices of G^{RS} coincide with the values $d_o + 3$ [Eqs. (26) and (35)], one more condition must be satisfied, namely, that the external field at each monomer is the same, which is implied in Eq. (2). This assumption is rigorously correct only for small clusters ($R_c \ll \lambda$). The present theory can be applicable to the clusters with $R_c \gg \lambda$ only if the far-field zone [i.e., monomers positioned at distances $r_{ij} \gg \lambda$ from a given ith one) contributes negligibly to the local field $\mathbf{E}_i$. The condition for this has been found in Ref. 17 to be

$$|X| \gg \begin{cases} (R_0/\lambda)^{3-D} & \text{for } D < 2 \\ (R_0/\lambda) N^{1-2/D} & \text{for } D > 2 . \end{cases} \tag{40}$$

Note that for the most common case of $D < 2$, the first of conditions (40) supersedes (39). If this is met, then the far-field zone (which might otherwise bring about interference phenomena) can be neglected. In the intermediate zone ($r_{ij} \sim \lambda$) the external field $\mathbf{E}^{(0)}$ is, strictly speaking, not constant, but does not change phase often enough to cause destructive interference. Therefore, in the zeroth-order approximation, we may neglect the variation of $\mathbf{E}^{(0)}$ and use Eq. (2).

Let us briefly recapitulate and discuss the analytical results obtained above. The enhancement factor of Raman scattering G^{RS} for each of the cases of large and small Stoke shifts [see Eqs. (26) and (35), (36), respectively] has the form of a power law in the variable X, with the corresponding index determined by the optical spectral dimension d_o, provided X is within the region given by Eq. (12). For the case of large shifts, this result is rigorously shown to be asymptotically exact, with an index equal to $1 + d_o$. For small Stokes shifts, scale invariance of G^{RS} is assumed [this assumption is strongly supported by the results of numerical simulation (see below)], and then the index $3 + d_o$ is obtained. Both the indices mentioned above are positive, implying that the enhancement increases with X. Physically, this property follows from the decrease of the eigenmode coherence length L_X [see Eq. (13)], which brings about enhancement of the local field fluctuations (from one monomer to another) in the fractal.

The Raman-scattering enhancement factor G^{RS} is found to be large, proportional to large factors, namely Q for the case of small and Q^3 for large Stokes shifts. Note that Q is required to be a large quantity as a necessary condition for the very existence of the scaling region [see Eq. (12)]. Thus strong enhancement of Raman scattering is characteristic of scaling and, consequently, of fractals consisting of monomers with high-quality optical resonances (i.e., with $Q \gg 1$), such as silver and gold fractal clusters.

The Raman-scattering intensity is proportional to the intensity (mean-squared magnitude) of the local fields induced on different monomers. Strong fluctuations of the local fields in fractals bring about an increased local field intensity and, consequently, enhanced Raman scattering. In a pure form this mechanism works for large Stokes shifts, in which case the scattered light does not interact with the cluster. Therefore the corresponding expression (25) G^{RS} simply coincides with the coefficient G of the enhancement of local fields found in Ref. 11.

Apart from the general mechanism discussed above, for the case of a small Stokes shift there exists an additional enhancement. The scattered field is not radiated freely, but rather interacts with the cluster. More exact-

ly, the dipole moment $\mathbf{d}^s$, induced at the shifted frequency ω_s, induces, in turn, secondary dipole moments at ω_s, and so on to self-consistency. The Raman radiation is emitted by the integral dipole moment $\mathbf{D}^s$ (22), resulting in an additional enhancement as given by Eq. (35). We point out that for the case of a small Stokes shift, G^{RS} (35) is certainly not the square of G^{RS} given by Eq. (26) for large Stokes shifts, as is often proposed in the SERS literature.

IV. NUMERICAL MODELING

We have examined two types of fractals, the random walk fractals [fractal dimension $D=2$ and optical spectral dimension $d_o \approx 0.4$ (Refs. 11 and 17)] and cluster-cluster aggregates[8] [$D \approx 1.7$ (Refs. 7 and 9) and $d_o \approx 0.3$ (Ref. 17)]. The clusters were generated using the Monte Carlo method and well-known procedures. Then, following Ref. 11, the clusters have been subjected to dilution (decimation), which consists of the following. The ith ($i=1,2,\ldots,N$) monomer is randomly retained in the cluster with some probability β, or removed with probability $1-\beta$. This procedure simplifies the fractal structure at small scales and reduces the total number N of monomers in the cluster on average by a factor β, simplifying greatly the numerical calculations. At the same time, the resulting (diluted) fractal is characterized by the same Hausdorff dimension as the original one. In most cases, 32-fold decimation ($\beta \approx 0.03$) has been performed. Some simulations have been done with β as small as 10^{-3} for comparison. The results of the computations clearly show that the optical properties of fractals in the scaling region [i.e., for X satisfying Eq. (12)] do not depend on the dilution, as expected. Finally, averaging over a large ensemble of fractals (up to 10^3) has been performed.

The enhancement factor G^{RS} of the cluster-enhanced Raman scattering is calculated accordingly to the exact expression (23) with the use of Eqs. (6) and (22). Most interesting from the experimental point of view is the case of small Stokes shifts, where G^{RS} is greatest. Also, because expression (26) for G^{RS} for the case of large Stokes shift is asymptotically exact, its properties are clear. It is for this reason that we concentrate below on the numerical modeling for the case of small Stokes shifts.

The theory [Eqs. (35) or (36)] predicts (i) scaling of G^{RS} as a function of the variable X with index d_o+3; (ii) proportionality of G^{RS} to Q^3; (iii) independence of G^{RS} from N; and (iv) equality of the scaling indices of G^{RS} for $X>0$ and $X<0$. The two last features are not self-evident. In fact, there are four summations over $n=1,2,\ldots,3N$ in the exact expression (30), and it is not clear *a priori* that these summations mutually cancel to result in the independence of G^{RS} from N. The equality of indices for $X>0$ and $X<0$ is not evident because Eqs. (2) and (16), along with all the solutions which follow from them, are not even with respect to the sign change $X \leftrightarrow -X$. The numerical computations strongly support these analytical results.

The normalized enhancement factor $G^{\mathrm{RS}}Q^{-3}$ for clusters generated assuming the cluster-cluster aggregation is shown in Fig. 1 as a function of the dimensionless spectral variable $R_0^3|X|$ for both positive and negative X (note the double-logarithmic scale). The calculated points lie along straight lines, indicating scaling of G^{RS} over seven decades of its magnitude. The scaling indices found from these data, 3.30 for $X>0$ and 3.27 for $X<0$, are almost equal and close to the predicted value of d_o+3 with the optical spectral dimension found in Ref. 17 of $d_o \approx 0.3$. The lines for $X>0$ and $X<0$ are parallel but not coincident, which shows that the coefficients, unlike the indices, are unequal (they differ by nearly a factor of 2). The last property results from the lack of symmetry with respect to the sign change of X, emphasizing the nontriviality of the equality of indices for $X>0$ and $X<0$.

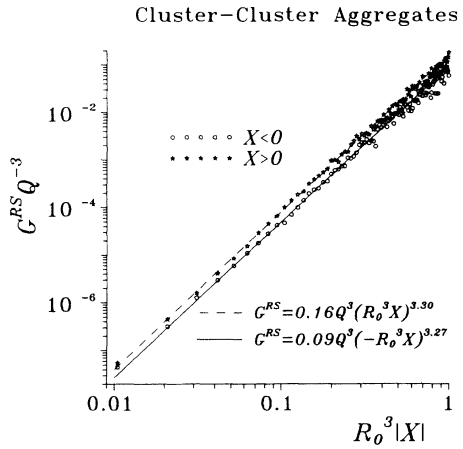

FIG. 1. The normalized enhancement factor for cluster-cluster aggregates plotted against the dimensionless spectral parameter ($R_0^3|X|$) in a double-logarithmic scale. The straight lines represent the best power-law fits to the data (the fit parameters are shown in the figure). The parameters used in the computations are $\beta=\frac{1}{32}$, $Q=200$, and $N=64$ (for notations see text). Each point is obtained by averaging over 250 individual clusters.

Further insight into the requirements for scaling and the test of the proportionality $G^{\mathrm{RS}} \propto Q^3$ is provided by Fig. 2, where $G^{\mathrm{RS}}Q^{-3}$ is plotted as a function of R_0^3X for

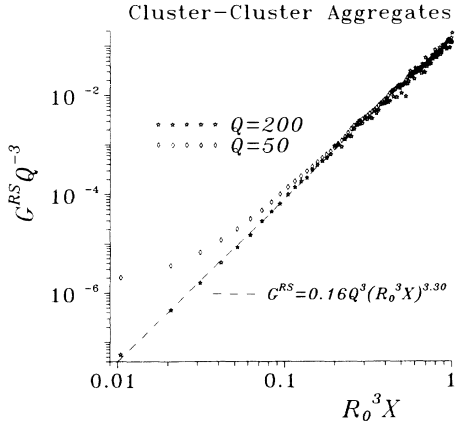

FIG. 2. The normalized enhancement factor $G^{\mathrm{RS}}Q^{-3}$ as a function of R_0^3X for two values of the resonance quality factor, $Q=200$ and 50. The rest of the parameters are the same as in Fig. 1.

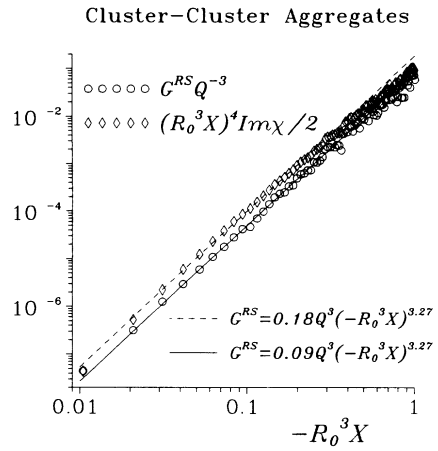

FIG. 3. The normalized enhancement factor $G^{RS}Q^{-3}$, computed with the exact formula (23) (circles) and approximation (36) (diamonds), plotted vs $-R_0^3X$ (for $X<0$) in a double-logarithmic scale. The straight lines correspond to the power-law fits with the parameters indicated in the figure. The clusters and parameters used in the computations are the same as in Fig. 1.

two different values of Q. We see that for $Q=200$ scaling takes place in the whole region presented in Fig. 2, while for $Q=50$ the scaling exists only when $R_0^3X \gtrsim 0.1$, where the two sets of data virtually coincide. This shows the importance of the scaling condition (12), which requires $XR_0^3 \gg Q^{-1}$. The independence of $G^{RS}Q^{-3}$ from Q in the region of scaling, clearly seen in Fig. 2, corroborates the analytical result that $G \propto Q^3$ in, and only in, this region.

Comparison of the results obtained from approximate formula (36) with the computations based on the exact expression (23) is presented in Fig. 3. We can see that the predictions of Eqs. (23) and (36) do not differ by more than a factor of 2 over seven decades, which makes Eq. (36) a useful approximation. The indices of the two sets of data are indeed very close, and a very good quantitative agreement is obtained if the numerical coefficient in Eq. (36) is changed from $\frac{1}{2}$ to $\frac{1}{4}$. The possible origin of the difference between the numerical coefficients is discussed at the end of the preceding section.

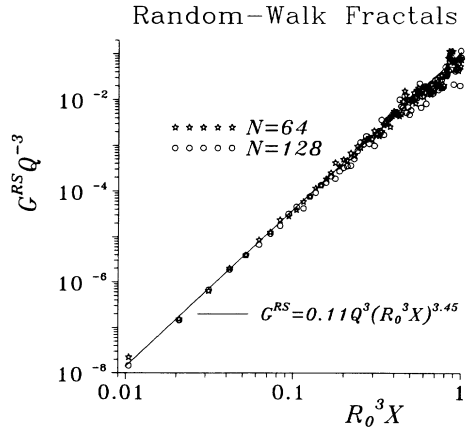

FIG. 4. The normalized enhancement factor $G^{RS}Q^{-3}$ for random walk fractals plotted vs R_0^3X (for $X>0$) in a double-logarithmic scale. The total number of monomers in a cluster is $N=128$ with averaging over 50 individual clusters (circles) and $N=64$ with averaging over 250 clusters (stars). The straight line corresponds to the best power-law fit with the parameters shown in the figure.

The data presented in Fig. 4 demonstrate scaling for random walk fractals, and also provide a direct test of independence of the enhancement coefficient G^{RS}, as defined by Eq. (23), from cluster size. The latter property is evident from Fig. 4, where the points corresponding to $N=64$ and 128 coincide within statistical error. The scaling is as good as for the case of Fig. 1, and the index found, 3.45, is reasonably close to the predicted value of $3+d_o$ with $d_o \approx 0.4$ as found in Refs. 11 and 17.

V. DISCUSSION

Since the analytical results obtained have been discussed at the end of Sec. III, we will mainly concentrate our discussion on the underlying physics and manifestation of the predicted critical behavior in observable optical phenomena, including quantitative comparison with experimental data.

Fractals are self-similar objects, and the general property of such objects is such that fluctuations in space on all scales are of the same relative magnitude. Therefore it is understandable that a mean-field approach is not applicable, and that the scaling behavior of linear optical responses takes place, as established in Ref. 11. The linear optical absorption and density of fractal eigenmodes scale with the same index d_o-1, where d_o is called the optical spectral dimension. This scaling is not present in terms of the frequency, but rather in terms of a "natural" spectral variable $X \equiv \mathrm{Re}\chi_0^{-1}$, where χ_0 is the optical polarizability of a single monomer. The variable X can be expressed in terms of light frequency ω or wavelength λ, but in a complicated, nonscaling form given below. The region of scaling is determined by Eq. (12) with additional conditions (39) and (40) for large ($R_c \gg \lambda$) clusters.

The main goal of this work is to examine how the scaling properties of the fractal, its eigenmodes and linear responses manifest themselves in the Raman scattering of light. The major result of this paper is the prediction of the scaling behavior of the enhancement factor G^{RS} of the Raman scattering. Before proceeding, let us recall that, by definition, the factor G^{RS} shows how many times the Raman intensity per monomer is increased upon aggregation of the monomers into a cluster. The Raman susceptibility of a monomer may represent either its own, inherent Raman scattering ability, or that of the adsorbates bound to it.

Physically, the intensity of Raman scattering is proportional to the averaged intensity of the local fields acting on the monomers in the cluster. Such a mechanism, acting in a pure form in the case of very large Stokes frequency shifts, predicts G^{RS} (25) to be equal to the enhancement factor G of the local fields, which has been

calculated[11] exactly earlier. In this case, the scaling of G^{RS} in X follows from the scaling of the optical absorption [$\mathrm{Im}\chi(X)$]. The magnitude of G^{RS} is large, proportional to the large parameter Q (quality factor of the optical resonance of monomers), and the scaling index is d_o+1.

In the case of a small Stokes shift, which is typical for most experiments (including those discussed below), the dynamic dipoles oscillating at the Stokes frequency interact with the fractal, resulting in additional enhancement of Raman scattering. In this case, G^{RS} (35) is much larger, proportional to Q^3, and the index is d_o+3. We note that the tentative theory of Raman-scattering enhancement based on the binary approximation (Ref. 10) predicts correctly the dependence of G^{RS} on Q, but fails to give the correct scaling in X.

The results of the numerical simulation presented above (Sec. IV) strongly support the scaling of G^{RS} in terms of X, the independence of G^{RS} from the number of monomers in the fractal, and the proportionality of G^{RS} to Q^3. Given the large values of Q characteristic of metal fractal clusters, the last feature qualitatively explains the strong enhancement of Raman scattering observed with aggregated colloidal metal clusters.

Now let us examine how the scaling relations established and discussed above translate into experimentally measurable spectral profiles of SERS, i.e., how G^{RS} depends on the wavelength λ. To do this, we need to know the variables X and δ as functions of λ. Let us concentrate on metallic fractal clusters. Such a cluster consists of aggregated spherical colloidal particles as monomers. The polarizability χ_0 of such a monomer is given by the familiar expression

$$\chi_0=R_m^3(\epsilon-\epsilon_0)(\epsilon+2\epsilon_0)^{-1}\ , \tag{41}$$

where R_m is the radius of the spherule, and ϵ and ϵ_0 are the dielectric permittivity of the colloidal material (metal) and embedding medium (usually water). From Eq. (41), the spectral variable X and the resonance quality factor $Q=1/R_0^3\delta$ are determined to be

$$X=-R_m^{-3}\frac{|2\epsilon+\epsilon_0|^2-9}{4|\epsilon-\epsilon_0|^2},\quad Q=\left[\frac{R_m}{R_0}\right]^3\frac{|\epsilon-\epsilon_0|^2}{3\epsilon''\epsilon_0}\ , \tag{42}$$

where $\epsilon''\equiv\mathrm{Im}\epsilon$.

From Eqs. (35), (41), and (42), we obtain an explicit expression for G^{RS} in terms of the metal dielectric permittivity ϵ,

$$G^{RS}\sim(R_0/R_m)^{3d_o}\frac{||\epsilon+\frac{1}{2}\epsilon_0|^2-\frac{9}{4}\epsilon_0|^{d_o+3}}{|\epsilon-\epsilon_0|^{2d_o}(3\epsilon''\epsilon_0)^3}\ . \tag{43}$$

Colloidal metal particles are known to be fractal clusters with the Hausdorff dimension close to that predicted[7,9] by the cluster-cluster aggregation model, $D\approx1.7$. For such clusters we can expect[17] $d_o\approx0.3$ and $R_0\sim R_m$. An electron micrograph of a silver colloidal cluster[18] is shown in Fig. 5. The cluster, which contains $\sim10^3$ metallic monomers, was produced as outlined in Ref. 19.

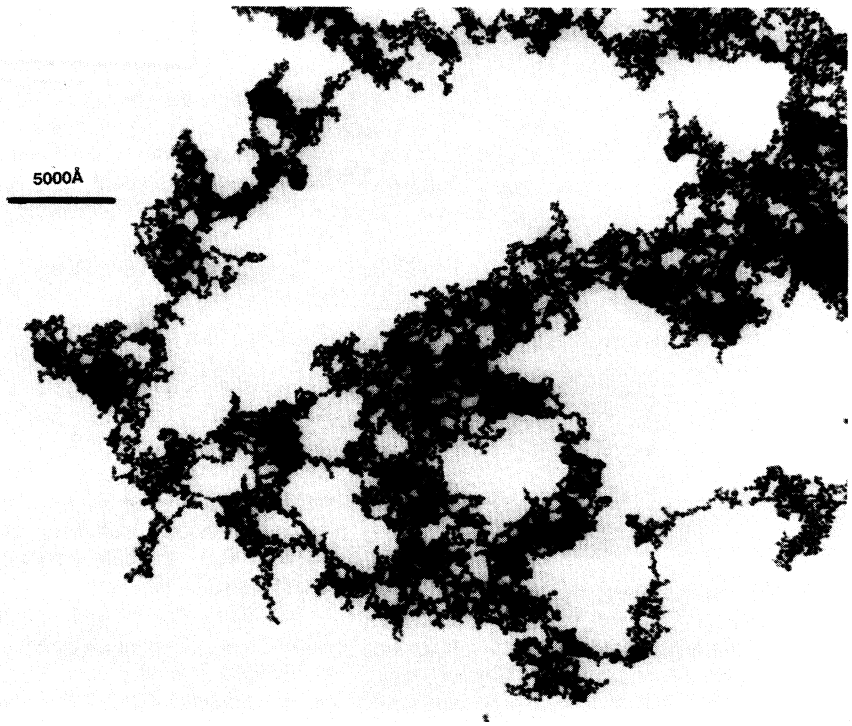

FIG. 5. Electron micrograph of a silver colloidal cluster, adopted from Ref. 18. For details of obtaining this, see Ref. 19.

One can clearly see in Fig. 5 the main qualitative feature of a fractal cluster, namely, its self-similarity on all spatial scales between the minimum scale (distance between monomers) and the maximum scale (total size of the cluster): each fragment after magnification resembles the whole cluster. Also, the tenuous structure of the cluster is evident: there are cavities of all sizes up to the total size of the cluster, and the larger the fragment that is considered, the lower its density.

In the red region of visible light, the dielectric constant $\epsilon' \equiv \mathrm{Re}\epsilon$ is known to be negative and large in magnitude for most metals, especially the noble metals, i.e., $-\epsilon' \gg \epsilon_0, \epsilon''$. In this case G^{RS} becomes very large,

$$G^{\mathrm{RS}} \sim \left[\frac{\epsilon'^2}{3\epsilon''} \right]^3 \sim Q^3 \gg 1 \ . \tag{44}$$

For noble metals, the resonance quality factor Q (42) can be as high as 100, yielding the upper estimate $G^{\mathrm{RS}} \sim 10^6$. Another role of the fractality is in the formation of the broad spectral contour of SERS displaying the dramatic increase from the blue to red region where Q is large.

The model with dipole-dipole interaction considered above does not include some factors present in real systems. In colloidal clusters, monomers are touching or almost touching each other (cf. Fig. 5). As a result of this, there may exist Ohmic conduction between the monomers. However, at high frequencies, the capacitive conductivity (which is taken into account by the dipole coupling) will prevail over the Ohmic conductivity, as argued in Ref. 11. Another factor is the short-range interactions of nearest monomers, namely, exchange and higher-multipole couplings (the exchange coupling is also responsible for conduction between the monomers). We believe that the long-range dipole interaction dominates in determining the collective excitation spectrum of a fractal, i.e., in the scaling region. However, the higher-multipole interactions may change the local fields acting on a monomer or on a monomer-adsorbed molecule, as has been shown[5] for two monomers. This factor can renormalize the magnitude of enhancement factor G^{RS}, but, probably, has lesser effect on its spectrum. We hope to return to quantitative consideration of these factors elsewhere.

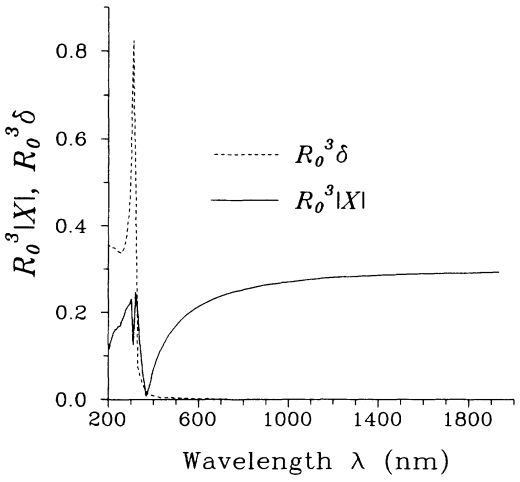

FIG. 6. Spectral parameter X and dissipation parameter δ, both multiplied by R_0^3 to give dimensionless quantities, plotted against wavelength λ. Optical constants for silver are taken from Ref. 20, and the ratio $R_0/R_m = 0.7$, typical for cluster-cluster aggregation, is assumed.

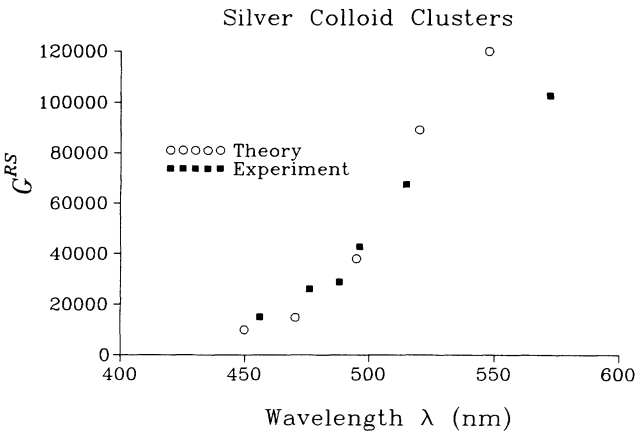

FIG. 7. Theoretical and experimental enhancement factors for the silver colloid clusters as functions of wavelength λ.

Let us compare the theory with experimental results obtained with colloidal silver. Figure 6 shows the spectral dependence of X and δ for silver calculated with optical constants adopted from Ref. 20. One can conclude from these data that the scaling region, where $X \gg \delta$, is $\lambda > 400$ nm. Also, in this region $Q = 1/R_0^3\delta$ is large.

Experimental SERS enhancement data obtained in Ref. 19 are compared in Fig. 7 with G^{RS} values calculated with Eq. (43) as a function of λ. Only the spectral dependence of G^{RS} is informative in this figure since only relative values of G^{RS} are reported in Ref. 19. The experimental data presented in Fig. 7 are normalized by setting $G^{\mathrm{RS}} = 15\,000$ at 460 nm, which is a reasonable value. Clearly, the present theory accounts successfully for the dramatic increase in Raman enhancement accompanying aggregation, and for the observed increase of G^{RS} towards the red despite the fact that the enhancement for a single silver colloidal particle is expected to peak in the near uv. We emphasize that, aside from a single multiplicable factor, the calculated enhancement factor contains no adjustable parameters (d_o has previously been found from modeling of linear responses).

ACKNOWLEDGMENTS

This research has been supported in part by the Office of Naval Research, and the National Science Foundation under Grant No. CHE-9196214. M.M. and V.M.S. thank NSERC and the Networks of Centres of Excellence for Molecular and Interfacial Dynamics for financial support.

*Also with the Institute of Automation and Electrometry, Siberian Branch of the Russian Academy of Sciences, 630090 Novosibirsk, Russia.

†Also with the L. V. Kirensky Institute of Physics, Siberian Branch of the Russian Academy of Sciences, 660036 Krasnoyarsk, Russia.

[1]*Surface-Enhanced Raman Scattering,* edited by R. K. Chang and T. E. Furtak (Plenum, New York, 1982).

[2]M. Moskovits, Rev. Mod. Phys. **57**, 783 (1985).

[3]P. F. Liao and A. Wokaun, J. Chem. Phys. **76**, 751 (1982).

[4]V. I. Emelyanov and N. I. Koroteev, Usp. Fiz. Nauk **135**, 345 (1981) [Sov. Phys. Usp. **24**, 864 (1981)].

[5]P. K. Aravind, A. Nitzan, and H. Metiu, Surf. Sci. **110**, 189 (1981).

[6]N. Liver, A. Nitzan, and J. J. Gersten, Chem. Phys. Lett. **111**, 449 (1984).

[7]D. A. Weitz and M. Oliveria, Phys. Rev. Lett. **52**, 1433 (1984).

[8]P. Meakin, Phys. Rev. Lett. **51**, 1119 (1983); M. Kolb, R. Botet, and R. Jullien, *ibid.* **51**, 1123 (1983).

[9]P. Meakin, J. Chem. Phys. **83**, 3645 (1985).

[10]V. M. Shalaev and M. I. Stockman, Zh. Eksp. Teor. Fiz. **92**, 509 (1987) [Sov. Phys. JETP **65**, 287 (1987)]; Z. Phys. D **10**, 71 (1988).

[11]V. A. Markel, L. S. Muratov, M. I. Stockman, and T. F. George, Phys. Rev. B **43**, 8183 (1991).

[12]M. I. Stockman, T. F. George, and V. M. Shalaev, Phys. Rev. B **44**, 115 (1991).

[13]S. Alexander and R. Orbach, J. Phys. (Paris) Lett. **43**, 625 (1982).

[14]B. Sapoval, Th. Gobron, and A. Margolina, Phys. Rev. Lett. **67**, 2794 (1991).

[15]S. Alexander, Phys. Rev. B **40**, 7953 (1989).

[16]For convenience, the notation is slightly changed from that of Ref. 11: here the eigenvector components $(i\alpha|n)$ correspond to the matrix elements $(i\alpha|U|n)$ of the diagonalizing operator in Ref. 11.

[17]V. M. Shalaev, R. Botet, and R. Jullien, Phys. Rev. B **44**, 12 216 (1991); **45**, 7592(E) (1992).

[18]J. S. Suh and M. Moskovits (unpublished).

[19]J. S. Suh and M. Moskovits, J. Phys. Chem. **58**, 5526 (1984).

[20]P. B. Johnson and R. W. Christy, Phys. Rev. B **6**, 4370 (1972).

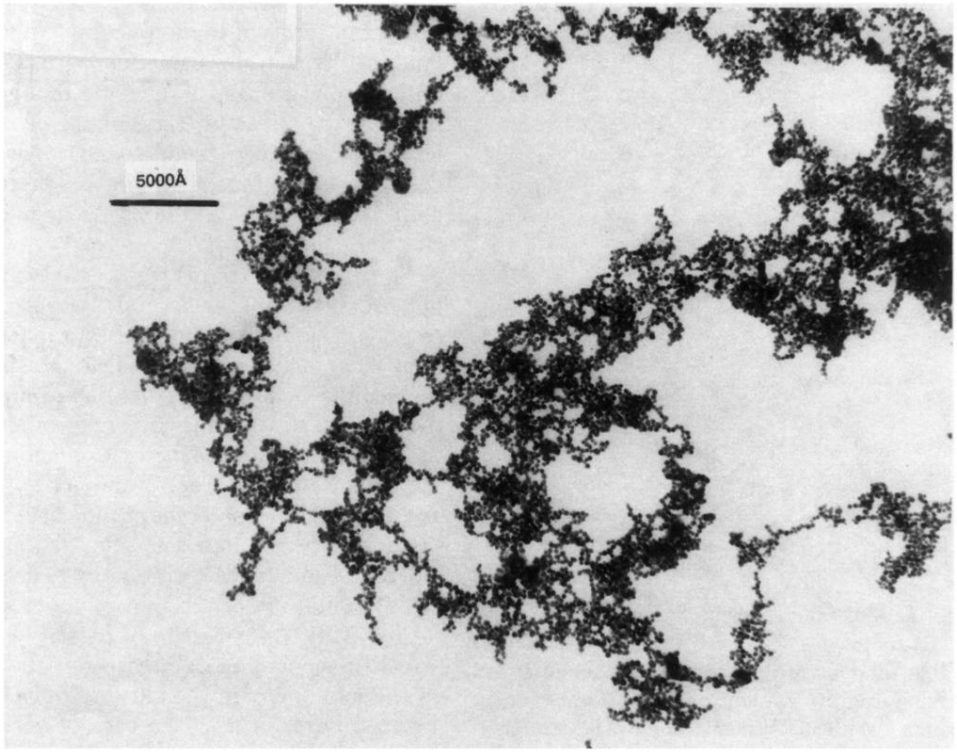

FIG. 5. Electron micrograph of a silver colloidal cluster, adopted from Ref. 18. For details of obtaining this, see Ref. 19.